Contents lists available at ScienceDirect

# Applied Catalysis B: Environmental

# Decolorization and mineralization of Sunset Yellow FCF azo dye by anodic oxidation, electro-Fenton, UVA photoelectro-Fenton and solar photoelectro-Fenton processes

Francisca C. Moreira [a], Sergi Garcia-Segura [b], Vítor J.P. Vilar [a], Rui A.R. Boaventura [a], Enric Brillas [b],*

[a] LSRE – Laboratory of Separation and Reaction Engineering – Associate Laboratory LSRE/LCM, Departamento de Engenharia Química, Faculdade de Engenharia, Universidade do Porto, Rua Dr. Roberto Frias, 4200-465, Porto, Portugal
[b] Laboratori d'Electroquímica dels Materials i del Medi Ambient, Departament de Química Física, Facultat de Química, Universitat de Barcelona, Martí i Franquès 1-11, 08028 Barcelona, Spain

A R T I C L E   I N F O

A B S T R A C T

The decolorization and mineralization of 100 mL of 290 mg L$^{-1}$ Sunset Yellow FCF (SY) azo dye at pH 3.0 were studied by anodic oxidation with electrogenerated $H_2O_2$ (AO-$H_2O_2$), electro-Fenton (EF), UVA photoelectro-Fenton (PEF) and solar photoelectro-Fenton (SPEF). Trials were performed in a one-compartment cell equipped with a boron-doped diamond (BDD) anode and a carbon–PTFE air-diffusion cathode. Organics were removed by hydroxyl radical ($^\bullet$OH) formed: (i) at the BDD anode from water oxidation, (ii) in the bulk from Fenton's reaction between added $Fe^{2+}$ and generated $H_2O_2$ at the cathode and (iii) from the photolysis of Fe(OH)$^{2+}$ species by UV light. The most powerful method was SPEF, achieving an almost total mineralization more rapidly than PEF due to the higher UV intensity of sunlight, which quickly photolyzes Fe(III)–carboxylate complexes that cannot be destroyed by $^\bullet$OH in EF. However, SY was completely decolorized at similar rate by EF, PEF and SPEF. The little oxidation action of $^\bullet$OH at the BDD anode yielded a slow decolorization and mineralization in AO-$H_2O_2$. The effect of current density on all treatments was examined. The azo dye decay always followed a pseudo-first-order reaction. It was more rapidly removed than decolorized, indicating that colored aromatic products are involved in the decolorization process. A total of 14 aromatic products and 34 hydroxylated derivatives, including benzenic, naphthalenic and phthalic acid compounds, were detected by LC–MS. Generated carboxylic acids like tartronic, oxalic, formic and oxamic were identified by ion-exclusion HPLC. The viability of SPEF at industrial scale was demonstrated using a solar pre-pilot plant with a Pt/carbon–PTFE air-diffusion cell coupled with a compound parabolic collectors (CPCs) photoreactor. In this plant, the treatment of 10 L of 290 mg L$^{-1}$ SY at pH 3.0 between 33.2 and 77.6 mA cm$^{-2}$ gave total decolorization and 91–94% mineralization in short time. A plausible general reaction sequence for SY mineralization involving all oxidation products detected was proposed.

© 2013 Elsevier B.V. All rights reserved.

## 1. Introduction

Synthetic dyes are extensively used for coloring textiles, leather, paper, food, drinks, pharmaceuticals, cosmetics and inks [1]. Azo dyes are by far the most important class of synthetic dyes, accounting for over 70% of all commercial dyes. They are characterized by one or more azo groups (—N=N—) as chromophore, with each group attached to two radicals of which at least one is aromatic containing functional groups such as —OH and —SO$_3$H, among others [2–4]. Large volumes of wastewaters with high azo dye contents are released by many industries and discharged into water bodies like lakes and rivers where they cause not only esthetic problems linked to wastewaters color, but also health risks on human beings and environmental damages by impeding the light penetration and due to toxicity, carcinogenicity, potential mutagenicity and resistance to biodegradation of these pollutants and their by-products [1,2,5]. Azo dyes persist in the aquatic environment due to their difficult removal under conventional treatments in wastewater treatment plants [3,6]. Research efforts are then needed for the development of powerful oxidation processes to destroy azo dyes and their by-products from wastewaters in order to avoid their adverse impact.

Among the different technologies tested for water remediation, electrochemical advanced oxidation processes (EAOPs) have recently received great attention by their environmental

compatibility, versatility, high efficiency, amenability of automation and safety owing to their use at mild conditions [7–10]. The great oxidation ability of these procedures to remove organic matter from waters is based on the in situ generation of hydroxyl radical ($\bullet$OH), which has so high standard reduction potential ($E°(\bullet OH/H_2O) = 2.80\,V/SHE$) that non-selectively reacts with most organics, giving dehydrogenated or hydroxylated products up to their mineralization, i.e., their transformation into $CO_2$, water and inorganic ions [9].

The most popular and simplest EAOP is anodic oxidation (AO), where organic pollutants are oxidized by direct electron transfer to the anode M and/or mediated oxidation with heterogeneous M($\bullet$OH) formed from water discharge at the anode surface at high current as follows [7,8,11,12]:

$$M + H_2O \rightarrow M(\bullet OH) + H^+ + e^- \qquad (1)$$

At present, the best anodic materials for AO are non-active boron-doped diamond (BDD) thin-film electrodes since they produce very high amounts of weakly adsorbed hydroxyl radicals (BDD($\bullet$OH)) from reaction (1) resulting in a much greater $O_2$-overpotential than other common anodes like Pt and $PbO_2$ [13,14] and in an enhancement of the removal of aromatics like azo dyes [15–21] and their generated carboxylic acids [22].

Other EAOPs based on Fenton's reaction chemistry like electro-Fenton (EF) and photoelectro-Fenton (PEF) have shown greater efficiency than AO [9]. The most spread setup for these methods includes an electrolytic cell where $H_2O_2$ is continuously generated in a contaminated acidic solution from the two-electron cathodic reduction of $O_2$ [9]:

$$O_{2(g)} + 2H^+ + 2e^- \rightarrow H_2O_2 \qquad (2)$$

Carbonaceous cathodes like graphite [23], carbon or graphite felts [24–28], carbon sponge [29], BDD [30,31], carbon–polytetrafluoroethylene (PTFE) gas ($O_2$ or air) diffusion [32–36], activated carbon fiber [37] and carbon nanotubes [38–40] have shown a high efficiency for $H_2O_2$ electrogeneration. In EF and PEF, low amounts of $Fe^{2+}$ ion are added to the solution as catalyst to react with electrogenerated $H_2O_2$ producing $\bullet$OH in the bulk, along with $Fe^{3+}$ ion, from Fenton's reaction with optimum pH of 2.8 [4]:

$$Fe^{2+} + H_2O_2 \rightarrow Fe^{3+} + \bullet OH + OH^- \qquad (3)$$
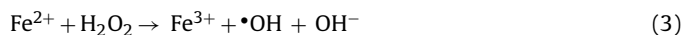
Note that EF is more efficient than the classical chemical Fenton process because reaction (3) can be mainly propagated by the cathodic reduction of $Fe^{3+}$ to $Fe^{2+}$ ion [9]:

$$Fe^{3+} + e^- \rightarrow Fe^{2+} \qquad (4)$$

In the EF treatment with a BDD anode using an undivided cell, the refractory organic molecules and their metal complexes can then be oxidized by the combined action of BDD($\bullet$OH) formed at the anode from reaction (1) and $\bullet$OH produced in the bulk from reaction (3).

Our research group also tested a carbon–PTFE gas ($O_2$ or air) diffusion cathode in the AO treatment (without $Fe^{2+}$ catalyst) of organics in an undivided cell with a BDD anode, thus developing the EAOP so-called AO with electrogenerated $H_2O_2$ (AO-$H_2O_2$) [32,41]. The high efficiency of this cathode to generate $H_2O_2$ from injected $O_2$ minimizes the possible cathodic reduction of organic pollutants. A quasi-steady content of $H_2O_2$ has been found in solution when its electrogeneration rate becomes equal to its destruction one, mainly due to its oxidation at the anode to $O_2$ via formation of hydroperoxyl radical (HO$_2\bullet$) as follows:

$$BDD + H_2O_2 \rightarrow BDD(HO_2\bullet) + H^+ + e^- \qquad (5)$$
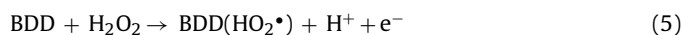
Under these conditions, it is expected that organics can be removed by reactive oxygen species (ROS) like BDD($\bullet$OH),

BDD(HO$_2\bullet$) and $H_2O_2$, although the former is the main oxidizing agent. Our group has reported that the EF treatment of aromatics does not yield total mineralization due to the formation of very stable by-products such as several Fe(III)–carboxylate complexes that react very slowly with generated M($\bullet$OH) and/or $\bullet$OH [31–33]. To solve this problem, the PEF process was introduced by us, which includes the simultaneous irradiation of the treated solution either with a UVA lamp or with inexpensive and renewable solar light, so-called solar PEF (SPEF). The catalytic action of UV light from both sources can be explained by two main processes [9,22,33,35,36,41–46]: (i) the photoreduction of Fe(OH)$^{2+}$, which is the predominant $Fe^{3+}$ species at pH near 3, regenerating more $Fe^{2+}$ ion and producing more $\bullet$OH, as shown in reaction (6), and (ii) the quick photolysis of Fe(III)–carboxylate complexes according to the general reaction (7):

$$Fe(OH)^{2+} + h\nu \rightarrow Fe^{2+} + \bullet OH \qquad (6)$$

$$Fe(OOCR)^{2+} + h\nu \rightarrow Fe^{2+} + CO_2 + R\bullet \qquad (7)$$
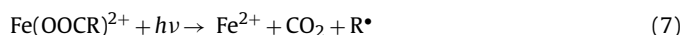
Only a limited number of papers have been published about the possible application of either PEF or SPEF to remove azo dyes and their by-products from acidic waters [37,44,46]. However, important aspects to clarify the viability of these processes like their comparative oxidation ability with AO-$H_2O_2$ and EF, the use of different anodes, the reactions producing aromatic intermediates and the influence of generated oxidants and UVA light on final by-products, have not been well checked yet. In this way, the mineralization of Sunset Yellow FCF azo dye (SY, see chemical formula and characteristics in Table 1) was carefully assessed by several EAOPs. SY is widely used as colorant in food, drugs and cosmetics [47]. Several papers have reported its removal, monitored spectrophotometrically by absorbance measurements, using $H_2O_2$ [48], peroxodisulfate in the absence and presence of Ag(I) [49], photocatalysis with transition metal complexes and $H_2O_2$ [50] and solar photo-Fenton with copper loaded bentonite [51]. An EF treatment for SY assessed in terms of decolorization, chemical oxygen demand (COD) and its content decay using a Pt anode and a reticulated vitreous carbon cathode has also been described [52].
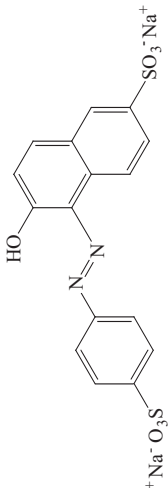
The present paper reports the results obtained for the comparative degradation of 290 mg L$^{-1}$ of commercial SY in acidic medium by AO-$H_2O_2$, EF, PEF and SPEF processes using a 100 mL BDD/carbon–PTFE air-diffusion cell. The SPEF degradation was also tested using a 10 L solar pre-pilot plant equipped with a Pt/carbon–PTFE air-diffusion cell coupled to compound parabolic collectors (CPCs) to clarify the effect of the anode and its viability. The influence of current density ($j$) on the decolorization rate and mineralization degree was examined for all processes. The SY decay and the evolution of generated carboxylic acids were followed by high-performance liquid chromatography (HPLC) to explain the role of $\bullet$OH and UV radiation during the mineralization processes. Aromatic intermediates were identified by liquid chromatography–mass spectrometry (LC–MS). A general reaction sequence for SY mineralization involving all detected products was finally proposed.

## 2. Experimental

### 2.1. Chemicals

Sunset Yellow FCF (81% purity and 19% of stabilizing inorganic salts) was of reagent grade supplied by Sigma–Aldrich. Tartronic, formic, oxalic and oxamic acids were of analytical grade purchased from Merck and Avocado. Anhydrous sodium sulfate, used as background electrolyte, and heptahydrated iron (II) sulfate, used as catalyst, were of analytical grade purchased from Merck and Fluka, respectively. For the assays in the 100 mL cell, solutions were

**Table 1**
Chemical structure and characteristics of Sunset Yellow FCF (SY) azo dye.

| Chemical structure | Chemical formula | Chemical name | Color index name | Color index number | Other names | $\lambda_{max}$ (nm) | $M$ (g mol$^{-1}$) |
|---|---|---|---|---|---|---|---|
| (structure shown) | $C_{16}H_{10}N_2Na_2O_7S_2$ | Disodium 6-hydroxy-5-[(4-sulfophenyl)azo]-2-naphthalene-sulfonate | Food Yellow 3 | 15,985 | Sunset Yellow FCF; Orange Yellow S; FD&C Yellow No.6; E110 | 482 | 452.37 |

prepared with ultrapure water obtained from a Millipore Milli-Q system, with resistivity > 18 MΩ cm at 25 °C, whereas the solutions treated in the 10 L solar pre-pilot plant were prepared with deionized water. The solution pH was adjusted using analytical grade sulfuric acid supplied by Acros Organics and sodium hydroxide supplied by Panreac. All the other chemicals were either of ultra-gradient grade for LC–MS, HPLC grade or analytical grade supplied by Acros Organics, Fluka, Lancaster, Merck, Panreac, Scharlau and Sigma–Aldrich.

## 2.2. Electrolytic systems

Laboratory scale electrolytic trials were conducted in an open, undivided and truncated conical glass BDD/air-diffusion cell of 100 mL equipped with a cooling jacket to ensure a constant temperature. The selected temperature was 35 °C, which is the maximum value established for this cell without significant water evaporation [53]. The characteristics of this system operating at constant $j$ are described in Supplementary material. Before use, the electrodes were polarized in 100 mL of 0.05 M $Na_2SO_4$ at pH 3.0 and 100 mA cm$^{-2}$ for 180 min to remove the impurities of the BDD anode surface and activate the air-diffusion cathode [54].

Comparative degradations of 100 mL of 290 mg L$^{-1}$ SY (100 mg L$^{-1}$ of total organic carbon (TOC)) in 0.05 M $Na_2SO_4$ as background electrolyte at pH 3.0 were performed by AO-$H_2O_2$, EF, PEF and SPEF processes. For the three latter EAOPs, 0.5 mM $Fe^{2+}$ was added to the solution as catalyst. The solution pH and $Fe^{2+}$ concentration were chosen since they were found optimal for analogous treatments of other aromatics [41,43–46]. The effect of $j$ in the range 16.7–100 mA cm$^{-2}$ on the oxidation power of each treatment was examined. In the PEF trials, the solution was irradiated with a Philips TL/6W/08 fluorescent black light blue tube placed at the top of the glass cell. It emitted UVA light in the wavelength region 320–400 nm with $\lambda_{max} = 360$ nm, yielding a photoionization energy of 5 W m$^{-2}$ as detected with a Kipp & Zonen CUV 5 global UV radiometer. In SPEF test, the cell was directly exposed to solar radiation with a mirror at its bottom to better collect the sun rays. All experiments were carried out under vigorous stirring with a magnetic bar at 700 rpm to ensure mixing and transport of reactants toward/from the electrodes.

Trials performed at pre-pilot scale were conducted in a 10 L flow plant equipped with a Pt/air-diffusion filter-press cell coupled with solar CPCs operating at constant $j$, 35 °C and in batch mode. A scheme of this system has been reported elsewhere [45] and its characteristics are reported in Supplementary material. The oxidation ability of this plant was studied by electrolyzing a 290 mg L$^{-1}$ SY solution in 0.05 M $Na_2SO_4$ with 0.5 mM $Fe^{2+}$ at pH 3.0 and $j$ values of 33.2, 55.4 and 77.6 mA cm$^{-2}$. Before using the plant for dye degradation, the air-diffusion cathode was activated by electrolyzing 10 L of 0.05 M $Na_2SO_4$ at pH 3.0 and 33.2 mA cm$^{-2}$ for 240 min.

All the SPEF experiments were run from the noon to 17 h as maximal in sunny and clear days during June–July 2012 in the research's group laboratory in Barcelona, Spain (latitude: 41°21′N; longitude: 2°10′E). The average solar UV radiation intensity (between 300 and 400 nm) was 28–30 W m$^{-2}$, as measured with the Kipp & Zonen CUV 5 global UV radiometer.

## 2.3. Apparatus and analytical procedures

The solution pH was determined using a Crison pH 25 portable pH meter. Samples were collected at regular time intervals and before analysis they were alkalinized to stop the mineralization process and filtered with 0.45 μm PTFE filters from Whatman. The decolorization of SY solutions was monitored by the decrease of their absorbance ($A$) at the maximum visible wavelength of $\lambda_{max} = 482$ nm (see Table 1), recorded on a Shimadzu 1800 UV–vis

spectrophotometer. Aliquots were always diluted 1:5 times and analyzed between 200 and 800 nm at 35 °C. The percentage of color removal or decolorization efficiency was calculated as follows [4,55]:

$$\% \, \text{Color removal} = \frac{A_0 - A_t}{A_0} \times 100 \tag{8}$$

where $A_0$ and $A_t$ are the absorbance at initial time and time $t$ at $\lambda_{max} = 482$ nm, respectively.

The mineralization of the dye solutions was assessed from their TOC abatement, determined on a Shimadzu VCSN TOC analyzer. Reproducible TOC values with an accuracy of $\pm 1\%$ were obtained by injecting 50 μL aliquots into the analyzer. Total nitrogen (TN) in solution was measured with the same TOC analyzer coupled with a Shimadzu TNM-1 unit. From TOC decay, the energy consumption per unit TOC mass ($EC_{TOC}$, in kWh $(\text{kg TOC})^{-1}$) and per unit volume ($EC$, in kWh m$^{-3}$) for the trials made in the 10 L pre-pilot plant were obtained from Eqs. (9) and (10), respectively [9,44]:

$$EC_{TOC} = \frac{1000 \, E_{cell} \, I \, t}{V_s \, \Delta(\text{TOC})_{exp}} \tag{9}$$

$$EC = \frac{E_{cell} \, I \, t}{V_s} \tag{10}$$

where 1000 is a conversion factor (mg g$^{-1}$), $E_{cell}$ is the average potential difference of the cell (V), $I$ is the applied current (A), $t$ is the electrolysis time (h), $V_s$ is the solution volume (L) and $\Delta(\text{TOC})_{exp}$ is the experimental TOC decay (mg L$^{-1}$).

The chromatographic parameters to determine the dye decay and the evolution of generated carboxylic acids and released inorganic ions are given in Supplementary material. Similarly, the LC–MS parameters used to identify the aromatic intermediates formed between 10 and 15 min of EF treatment of 100 mL of a 290 mg L$^{-1}$ SY solution in a BDD/carbon–PTFE air-diffusion cell at 33.3 mA cm$^{-2}$ are reported in Supplementary material.

### 2.4. Model parameters estimation

A pseudo-first-order kinetic model was fitted to the experimental data using a nonlinear regression method calculated from Fig.P software for Windows from Biosoft. The pseudo-first-order rate constants for decolorization at $\lambda_{max} = 482$ nm ($k_1(\text{dec})$, in min$^{-1}$) and for SY concentration decay ($k_1(\text{SY})$, in min$^{-1}$) were calculated from Eqs. (11) and (12), respectively:

$$A_t = A_0 \, e^{-k_1(\text{dec})t} \tag{11}$$

$$[\text{SY}]_t = [\text{SY}]_0 \, e^{-k_1(\text{SY})t} \tag{12}$$

where $[\text{SY}]_0$ and $[\text{SY}]_t$ are the SY concentration at initial time and time $t$, respectively. The initial TOC removal rate ($r_0(\text{TOC})$, in mg L$^{-1}$ min$^{-1}$) was obtained as follows:

$$r_0(\text{TOC}) = k_1(\text{TOC}) \times \text{TOC}_0 \tag{13}$$

where $k_1(\text{TOC})$ (in min$^{-1}$) is the pseudo-first-order rate constant for TOC removal given by $\text{TOC}_t = \text{TOC}_0 \, e^{-k_1(\text{TOC})t}$, in which $\text{TOC}_0$ and $\text{TOC}_t$ are the TOC concentration at initial time and time $t$, respectively. The resulting kinetics parameters were found by minimizing the sum of the squared deviations between experimental and predicted values. The goodness of all these parameters was assessed by calculating relative standard deviations, square of the correlation coefficient ($R^2$) and residual variance ($S_R^2$).
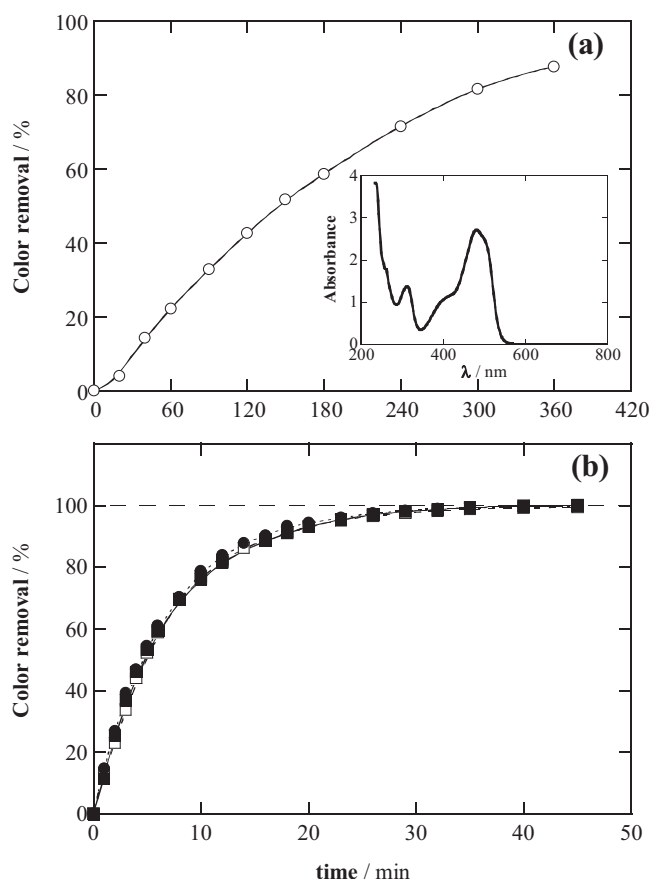


**Fig. 1.** Percentage of color removal at $\lambda_{max} = 482$ nm with electrolysis time for the degradation of 100 mL of 290 mg L$^{-1}$ Sunset Yellow FCF (SY) solutions in 0.05 M Na$_2$SO$_4$ at pH 3.0, 33.3 mA cm$^{-2}$, 35 °C under stirring at 700 rpm. Electrolytic trials were made in an undivided cell containing a boron-doped diamond (BDD) anode and a carbon–PTFE air-diffusion cathode, both of 3 cm$^2$ area. In plot (a), (○) anodic oxidation with electrogenerated H$_2$O$_2$ (AO-H$_2$O$_2$). The inset panel shows the UV–vis absorption spectrum of the initial SY solution diluted 1:5. In plot (b), (□) electro-Fenton (EF) with 0.5 mM Fe$^{2+}$, (●) photoelectro-Fenton (PEF) with 0.5 mM Fe$^{2+}$ under a 6 W UVA irradiation of $\lambda_{max} = 360$ nm and (■) solar PEF (SPEF) with 0.5 mM Fe$^{2+}$ under sunlight irradiation.

## 3. Results and discussion

### 3.1. Comparative degradation of SY by EAOPs in the 100 mL cell

The degradation of SY by AO-H$_2$O$_2$, EF, PEF and SPEF in the 100 mL cell was comparatively assessed by electrolyzing 290 mg L$^{-1}$ of the azo dye in 0.05 M Na$_2$SO$_4$ at pH 3.0, 33.3 mA cm$^{-2}$ and 35 °C, with addition of 0.5 mM Fe$^{2+}$ for the three latter EAOPs. In these trials, the solution pH decreased slowly to pH 2.4–2.7, probably due to the formation of carboxylic acids [41,43], and for this reason it was regularly adjusted to its initial value by adding small volumes of 0.5 M NaOH. As can be seen in the inset panel of Fig. 1a, the UV–vis spectrum of the initial solution (diluted 1:5) shows a strong visible band with $\lambda_{max} = 482$ nm (characteristic of SY, see Table 1), along with a much weaker shoulder near 420 nm. According to the behavior of other similar azo dyes [56], these bands can be associated with two tautomeric forms in equilibrium, the hydrazone form, where the hydroxyl group appears as carbonyl group and its hydrogen is linked to the azo group, and the azo one (presented in Table 1). The hydrazone form is expected to yield the stronger band at $\lambda_{max} = 482$ nm [56] and then predominates over the azo form that gives the weak shoulder at 420 nm. In addition, the UV–vis spectrum of Fig. 1a exhibits a weak band in the UV region centered at 314 nm due to the naphthalene group of SY [56], but it
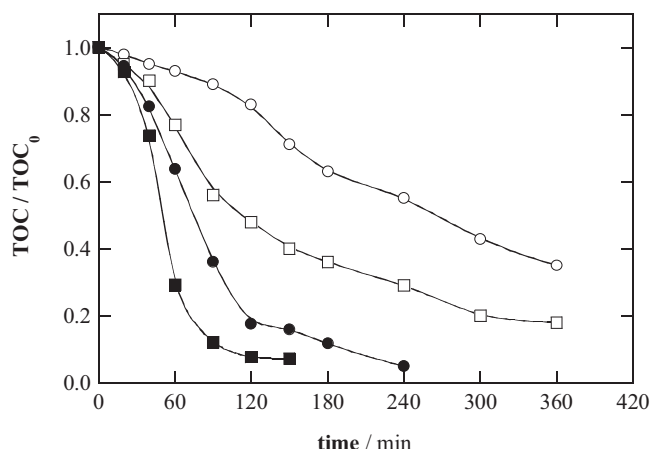
**Fig. 2.** Change of normalized TOC with electrolysis time for the treatment of 100 mL of 290 mg L$^{-1}$ SY solutions under the same conditions of Fig. 1. Method: (○) AO-H$_2$O$_2$, (□) EF, (●) PEF and (■) SPEF.

does not display clearly the band related to the benzene group, expected at about 240 nm, because it overlaps with the band of high absorbance recorded up to $\lambda = 280$ nm. Based on this, the decolorization efficiency for SY by the EAOPs tested was determined from the absorbance decay at $\lambda_{max} = 482$ nm using Eq. (8).
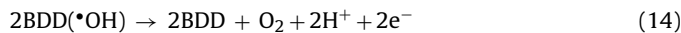
Fig. 1a highlights that the AO-H$_2$O$_2$ process only allowed a slow decolorization, reaching 88% color removal in 360 min. The initial orange solution lost gradually intensity to attain a light orange color at the end of this treatment. That means that SY and its conjugated aromatic products react very slowly with BDD($^\bullet$OH) formed from reaction (1) limited by their mass transfer to the anode, as well as with other weaker ROS (H$_2$O$_2$, BDD(HO$_2$$^\bullet$)). Note that analogous color removals were found by stirring the solution with the magnetic bar at rotating rates > 400 rpm, indicating that the AO-H$_2$O$_2$ process was controlled by mass transfer. In contrast, Fig. 1b evidences a similar and much quicker color removal when EF, PEF and SPEF were tested. In these three treatments, the initial solution already reached over 50% color removal during the first 5 min of electrolysis. At longer time, it acquired a brown color, probably due to the fast formation of great amounts of initial conjugated aromatic products, which are rapidly oxidized becoming the solution colorless in 40–45 min. This behavior indicates that in EF, PEF and SPEF, the azo dye and its conjugated aromatic products are mainly destroyed by $^\bullet$OH produced from Fenton's reaction (3), with a small participation of the photolytic reaction (6) induced by UVA light or sunlight.

Table 2 collects the $k_1$(dec) values, along with the corresponding $R^2$ and $S_R^2$, obtained for the four EAOPs tested. Quite similar $k_1$(dec) values for EF, PEF and SPEF can be observed, which are about 30 times higher than $k_1$(dec) for AO-H$_2$O$_2$, as expected if in the three former methods it is produced much higher amounts of $^\bullet$OH in the bulk than of BDD($^\bullet$OH) at the anode surface.

A very different behavior was found when TOC abatement was measured for the above trials. Fig. 2 shows that the oxidation power of EAOPs on the SY solution increases in the sequence: AO-H$_2$O$_2$ < EF < PEF < SPEF. The AO-H$_2$O$_2$ method led to a very poor TOC removal, only attaining 65% mineralization at 360 min, owe to the little oxidation action of BDD($^\bullet$OH) and other generated ROS, as stated above. In EF, the higher oxidation ability of additional $^\bullet$OH produced from Fenton's reaction (3) allowed a quicker TOC decay up to 82% mineralization. Note that at times longer than 120 min the EF process is progressively decelerated, probably due to the formation of Fe(III)–carboxylate complexes that are hardly oxidized by $^\bullet$OH [22,41,44]. This point was confirmed in the PEF process, where the fast photolysis of these complexes under UVA radiation

via reaction (7) can explain the almost total mineralization with 95% TOC removal reached at 240 min. Fig. 2 also shows that the azo dye underwent even a quicker degradation using SPEF with 93% TOC decay in only 150 min, which can be ascribed to the more rapid photodegradation of Fe(III)–carboxylate complexes induced by the more potent UV intensity supplied by sunlight. Be aware that in PEF and SPEF the additional action of $^\bullet$OH produced from photolytic reaction (6) could also accelerate the destruction of organics, although it has little influence on decolorization (see Fig. 1b). The fact that the solution is very slowly mineralized at long electrolysis time of these two EAOPs suggests the presence of hardly oxidizable final by-products that can only react slowly with BDD($^\bullet$OH), but neither destroyed with $^\bullet$OH nor photodecomposed, as will be better discussed below.

The applied $j$ is a key factor in the oxidation ability of EAOPs because it regulates the amounts of $^\bullet$OH acting as oxidizing agents. The effect of this experimental variable was checked by electrolyzing the above 290 mg L$^{-1}$ SY solution for each treatment at 16.7, 33.3 and 100 mA cm$^{-2}$ for 120–360 min. In all cases, TOC was faster destroyed with raising $j$. This tendency can be easily deduced from the $r_0$(TOC) values determined for all trials and summarized in Table 3. An inspection of this table corroborates that $r_0$(TOC) increased with raising $j$ for each EAOP and SPEF was always the most powerful treatment. In addition, greater $j$ also caused an acceleration of the degradation yielding higher mineralization degree at given time. For example, after 120 min of SPEF treatment, increasing TOC decays of 76%, 92% and 97% were found for increasing $j$ values of 16.7, 33.3 and 100 mA cm$^{-2}$, respectively. The faster mineralization observed for all EAOPs at higher $j$ can be simply related to the concomitant production of more oxidant $^\bullet$OH, due to the acceleration of reaction (1) to yield larger quantities of BDD($^\bullet$OH) and/or of Fenton's reaction (3) to give greater amounts of $^\bullet$OH as a result of the faster cathodic generation of H$_2$O$_2$ [41]. However, the opposite tendency was found when TOC removal was plotted against the consumed specific charge ($Q$, in Ah L$^{-1}$). Fig. 3a–d presents the normalized TOC vs. $Q$ for the AO-H$_2$O$_2$, EF, PEF and SPEF trials. A spent of more specific charge with raising $j$ can be observed in all cases, more apparent when $j$ changes from 33.3 to 100 mA cm$^{-2}$. This loss in efficiency can be accounted for by the generation of less relative amounts of $^\bullet$OH owing to the higher increase in rate of their non-oxidizing waste reactions, thereby lowering the organic events. These parasitic reactions involve primordially the oxidation of BDD($^\bullet$OH) to O$_2$ at the anode by reaction (14), the dimerization of $^\bullet$OH to H$_2$O$_2$ in the bulk by reaction (15) and the destruction of this radical either with H$_2$O$_2$ generating HO$_2$$^\bullet$ by reaction (16) or with Fe$^{2+}$ by reaction (17) [4,8,9,24]:

$$2BDD(^\bullet OH) \rightarrow 2BDD + O_2 + 2H^+ + 2e^- \tag{14}$$

$$2^\bullet OH \rightarrow H_2O_2 \tag{15}$$

$$H_2O_2 + {}^\bullet OH \rightarrow HO_2^\bullet + H_2O \tag{16}$$

$$Fe^{2+} + {}^\bullet OH \rightarrow Fe^{3+} + OH^- \tag{17}$$

Note that in EF and PEF, the destruction of H$_2$O$_2$ by $^\bullet$OH from reaction (16) is rather insignificant and H$_2$O$_2$ is always accumulated in the treated solution due to their efficient generation at the gas-diffusion cathode, thereby providing the maximum concentration of $^\bullet$OH from Fenton's reaction (3) to oxidize the organic pollutants [9,41].

The aforementioned results indicate that SPEF is the most powerful treatment for SY degradation, although EF and PEF yield similar decolorization efficiency. Greater $j$ accelerates the mineralization process, but it is preferable the use of low $j$ values to enhance the efficiency due to the smaller effect of waste reactions of $^\bullet$OH. The role of these oxidants, UVA light and sunlight in the treatments

**Table 2**
Pseudo-first-order rate constants for decolorization at $\lambda_{max} = 482$ nm ($k_1$(dec)) and for SY concentration decay ($k_1$(SY)), along with the corresponding square of the correlation coefficient ($R^2$) and residual variance ($S_R^2$), obtained for the treatment by different EAOPs of 100 mL of 290 mg L$^{-1}$ SY solutions in 0.05 M Na$_2$SO$_4$ at pH 3.0 and 35 °C using a BDD/carbon–PTFE air-diffusion cell and for the SPEF treatment of 10 L of the same solution in a pre-pilot plant equipped with a Pt/carbon–PTFE air-diffusion cell coupled with a CPCs photoreactor.

| Method | Current density (mA cm$^{-2}$) | $k_1$(dec)$^a$ (min$^{-1}$) | $R^2$ | $S_R^2$ | $k_1$(SY)$^b$ (min$^{-1}$) | $R^2$ | $S_R^2$ (mg$^2$ L$^{-2}$) |
|---|---|---|---|---|---|---|---|
| *100 mL cell* | | | | | | | |
| AO-H$_2$O$_2$ $^c$ | 33.3 | 0.0049 ± 0.0002 | 0.996 | 0.008 | 0.0083 ± 0.0002 | 0.993 | 34 |
| EF$^d$ | | 0.143 ± 0.001 | 0.999 | 0.001 | 0.149 ± 0.003 | 0.998$^d$ | 32 |
| PEF$^e$ | | 0.155 ± 0.001 | 1.000 | 0.000 | 0.170 ± 0.003 | 0.995 | 37 |
| SPEF$^f$ | | 0.146 ± 0.002 | 0.999 | 0.001 | 0.210 ± 0.002 | 0.995 | 61 |
| *10 L solar pre-pilot plant* | | | | | | | |
| SPEF$^f$ | 33.2 | 0.055 ± 0.003 | 0.994 | 0.007 | –$^g$ | –$^g$ | –$^g$ |
| | 55.4 | 0.069 ± 0.005 | 0.993 | 0.004 | –$^g$ | –$^g$ | –$^g$ |
| | 77.6 | 0.100 ± 0.004 | 0.993 | 0.005 | 0.191 ± 0.002 | 0.999 | 13 |

$^a$ Determined from Eq. (11).
$^b$ Determined from Eq. (12).
$^c$ Anodic oxidation with electrogenerated H$_2$O$_2$.
$^d$ Electro-Fenton with 0.5 mM Fe$^{2+}$.
$^e$ Photoelectro-Fenton with 0.5 mM Fe$^{2+}$ under a 6 W UVA irradiation of $\lambda_{max} = 360$ nm.
$^f$ Solar photoelectro-Fenton with 0.5 mM Fe$^{2+}$ under sunlight irradiation.
$^g$ Not determined.

**Table 3**
Effect of current density on the initial TOC removal rate ($r_0$(TOC)) along with the corresponding $R^2$ and $S_R^2$, obtained for the treatment of 290 mg L$^{-1}$ SY solutions in the 100 mL cell and in the 10 L solar pre-pilot plant by the same EAOPs of Table 2.

| Method | Current density (mA cm$^{-2}$) | $r_0$(TOC)$^a$ (mg C L$^{-1}$ min$^{-1}$) | $R^2$ | $S_R^2$ (mg$^2$ C L$^{-2}$) |
|---|---|---|---|---|
| *100 mL cell* | | | | |
| AO-H$_2$O$_2$ | 16.7 | 0.15 ± 0.01 | 0.986 | 7 |
| | 33.3 | 0.22 ± 0.02 | 0.974 | 24 |
| | 100 | 0.39 ± 0.02 | 0.987 | 12 |
| EF | 16.7 | 0.30 ± 0.01 | 0.988 | 17 |
| | 33.3 | 0.68 ± 0.04 | 0.975 | 26 |
| | 100 | 0.97 ± 0.07 | 0.976 | 25 |
| PEF | 16.7 | 1.1 ± 0.1 | 0.968 | 72 |
| | 33.3 | 1.5 ± 0.1 | 0.981 | 45 |
| | 100 | 1.9 ± 0.1 | 0.985 | 28 |
| SPEF | 16.7 | 1.9 ± 0.2 | 0.981 | 29 |
| | 33.3 | 2.3 ± 0.4 | 0.950 | 92 |
| | 100 | 3.5 ± 0.5 | 0.969 | 65 |
| *10 L solar pre-pilot plant* | | | | |
| SPEF | 33.2 | 1.0 ± 0.1 | 0.975 | 46 |
| | 55.4 | 1.6 ± 0.2 | 0.984 | 44 |
| | 77.6 | 1.8 ± 0.3 | 0.937 | 105 |

$^a$ Determined from Eq. (13).

tested was further examined from the SY concentration decay, as discussed in subsection below.

### 3.2. Decay kinetics for SY in the 100 mL cell

The reaction between the azo dye and oxidizing agents was followed by reversed-phase HPLC, where it exhibited a defined peak at retention time ($t_r$) of 5.4 min. No significant removal of SY was found in blank experiments performed with a 290 mg L$^{-1}$ SY solution in 0.05 M Na$_2$SO$_4$ at pH 3.0 and 35 °C with and without 20 mM H$_2$O$_2$ under UVA and solar radiation. This indicates that in the EAOPs tested, SY is mainly attacked by BDD($^\bullet$OH) and/or $^\bullet$OH, but not directly photolyzed. Note that $^\bullet$OH generation from H$_2$O$_2$ photolysis is negligible under sunlight irradiation ($\lambda > 300$ nm) since significant $^\bullet$OH yields are only obtained for short-wave UV irradiations (200–280 nm) [57].

Fig. 4 presents the decay of SY concentration for the treatment of 290 mg L$^{-1}$ dye solutions (corresponding to 235 mg L$^{-1}$ of pure SY) by all EAOPs at 33.3 mA cm$^{-2}$. Its inset panel evidences that the azo dye underwent a slow removal by AO-H$_2$O$_2$ until 95% disappearance at 360 min, as a result of its low reaction rate with BDD($^\bullet$OH). The use of EF accelerated strongly the SY removal, disappearing in 26 min, since it is much more rapidly attacked by $^\bullet$OH formed from Fenton's reaction (3). The SY destruction became much faster for

PEF, with total removal in 20 min, because of the additional production of $^\bullet$OH by photolytic reaction (6) induced with a 6 W UVA light, since it is not photolyzed. The alternative application of SPEF even led to a more rapid SY decay to disappear in only 16 min, owe to the greater generation of $^\bullet$OH also under the action of reaction (6), but induced by the higher UV intensity supplied by sunlight. All these findings corroborate that $^\bullet$OH formed from reactions (3) and/or (6) has much greater oxidation ability than BDD($^\bullet$OH) to remove the azo dye.

A pseudo-first-order kinetic model was able to fit well the above SY concentration decays, suggesting a constant production of BDD($^\bullet$OH) and/or $^\bullet$OH in each EAOP. The corresponding $k_1$(SY), along with their $R^2$ and $S_R^2$ values, are listed in Table 2. As expected, $k_1$(SY) rose in the order AO-H$_2$O$_2$ < EF < PEF < SPEF, in agreement with the increasing generation of $^\bullet$OH in the bulk. Results of Table 2 also evidence that $k_1$(SY) $\gg k_1$(dec) for all treatments. This means that decolorization involves the simultaneous destruction of the azo dye and some colored aromatic products that absorb at a wavelength similar to $\lambda_{max} = 482$ nm, being this process slower than SY removal alone. The longer persistence of such derivatives by the attack with $^\bullet$OH could explain the similar percentage of color removal (see Fig. 1b) and $k_1$(dec) values (see Table 2) found for EF, PEF and SPEF, contrasting with the different behavior for SY decay (see Fig. 4). The fast SY removal compared with the slow TOC
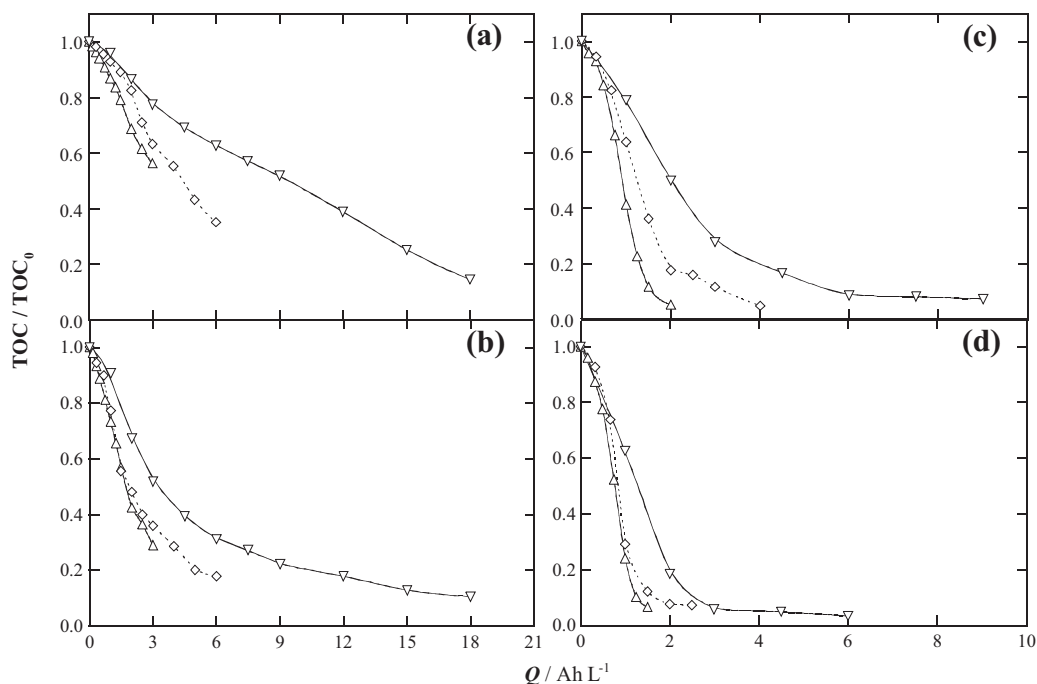
**Fig. 3.** Effect of current density on normalized TOC removal with consumed specific charge for the degradation of 100 mL of 290 mg L$^{-1}$ SY solutions in 0.05 M Na$_2$SO$_4$ at pH 3.0 and 35 °C in the BDD/carbon–PTFE air-diffusion cell by (a) AO-H$_2$O$_2$, (b) EF with 0.5 mM Fe$^{2+}$, (c) PEF with 0.5 mM Fe$^{2+}$ under a 6 W UVA irradiation of $\lambda_{max}$ = 360 nm and (d) SPEF with 0.5 mM Fe$^{2+}$. Applied current density: (△) 16.7 mA cm$^{-2}$, (◇) 33.3 mA cm$^{-2}$ and (▽) 100 mA cm$^{-2}$.

decay indicates the formation of more persistent oxidation products, which were identified by LC–MS and ion-exclusion HPLC, as described in subsection below.

### 3.3. Identification and evolution of oxidation products in the 100 mL cell

Since organics are mainly attacked by •OH, the same kind of oxidation products are expected in all EAOPs tested. Table 4 collects the 15 aromatic compounds, including the initial SY dianion (**1**), and 34 hydroxylated derivatives detected by LC–MS after 10–15 min of EF treatment at 33.3 mA cm$^{-2}$. As can be seen, the desulfonation of **1** yields the compounds **2** and **3**, whereas the cleavage of the −N=N− bond of these three aromatics leads to: (i) benzenic derivatives (compounds **4**–**7**) and (ii) naphthalenic derivatives (compounds

**8**–**11**), which are degraded to phthalic acid derivatives (compounds **12**–**15**). These reactions involve the oxidation of −NH$_2$ to −NO$_2$ group, deamination, denitration, hydroxylation, desulfonation and the breaking of the naphthalene moiety. Note that the hydroxylated compounds of **1**, as well as **2**, **3** and their hydroxylated compounds, are colored aromatics that are expected to absorb near $\lambda_{max}$ = 482 nm, and hence, their accumulation in the medium due to their lower reaction rate with •OH than SY could justify the longer time needed for decolorization compared with azo dye removal.

Ion-exclusion chromatograms of electrolyzed solutions at 33.3 mA cm$^{-2}$ revealed the generation of carboxylic acids like oxalic ($t_r$ = 7.0 min), tartronic ($t_r$ = 7.9 min), oxamic ($t_r$ = 9.3 min) and formic ($t_r$ = 13.8 min). Tartronic acid can be formed from the cleavage of the benzene and naphthalene rings of aromatic products and its further oxidation, as well as the degradation of other unidentified carboxylic acids, yields formic and oxalic acids [9,24,26,36,45]. Oxamic acid is expected to be formed from the destruction of N-intermediates with a −NH$_2$ group. Oxalic, formic and oxamic acids are ultimate acids since they are directly mineralized to CO$_2$ [22]. In EF, PEF and SPEF with a BDD/carbon–PTFE air-diffusion cell, these carboxylic acids are primordially present in solution as Fe(III)–carboxylate complexes because Fe$^{2+}$ ion is largely converted into Fe$^{3+}$ ion [9,22,46].

Fig. 5a depicts that tartronic acid is poorly accumulated (<1.5 mg L$^{-1}$) and slowly removed by BDD(•OH) in AO-H$_2$O$_2$, whereas in EF it is much more largely accumulated up to ca. 7 mg L$^{-1}$ after 135 min, disappearing at 360 min of electrolysis. The greater concentration achieved by this acid in the EF treatment can be related to the quicker degradation of precedent products by •OH and its fast decay indicates a high reaction rate of Fe(III)–tartronate complexes with •OH, mainly BDD(•OH) [9,22]. The faster photodecomposition of these complexes under UVA light accounts for by their quicker disappearance in PEF, which is accelerated in SPEF by the high intensity of UV radiation of sunlight. Fig. 5b highlights that oxalic acid is only accumulated up to ca. 1.1 mg L$^{-1}$ by AO-H$_2$O$_2$, attaining a concentration as high as 85 mg L$^{-1}$ at 150 min of EF, which only falls to 60 mg L$^{-1}$ at the end of electrolysis because of
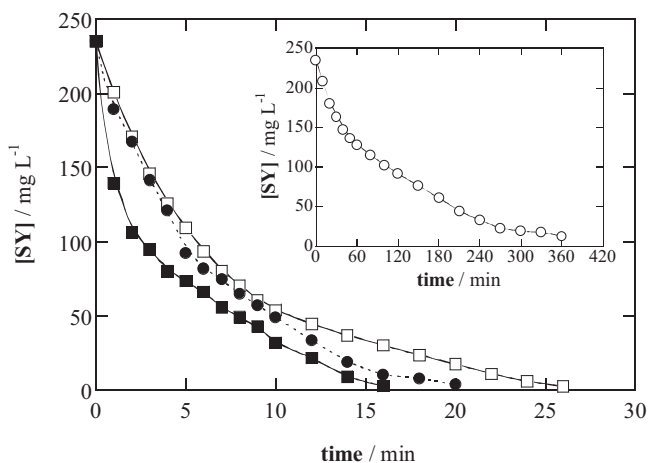


**Fig. 4.** Decay of SY concentration with electrolysis time for the degradation of 100 mL of a 290 mg L$^{-1}$ SY solution (235 mg L$^{-1}$ of pure SY) under the same conditions of Fig. 1. Method: (○) AO-H$_2$O$_2$, (□) EF, (●) PEF and (■) SPEF.

**Table 4**
Aromatic compounds and hydroxylated derivatives identified by LC–MS in negative mode during the EF treatment of 100 mL of a 290 mg L$^{-1}$ SY solution using a 100 mL BDD/carbon–PTFE air-diffusion cell.
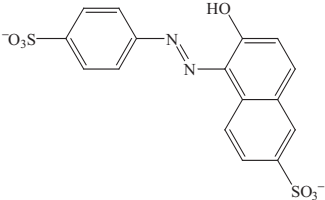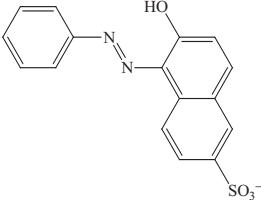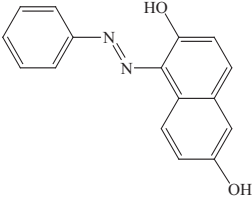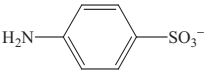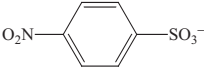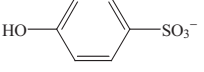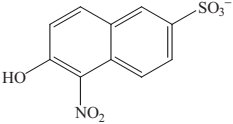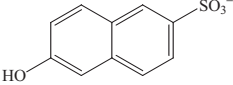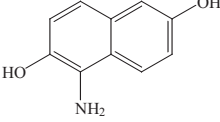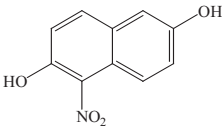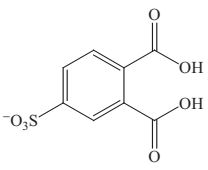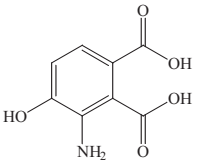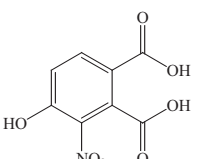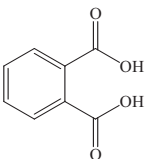
| Compound | Molecular formula | Number of –OH added | m/z | |
|---|---|---|---|---|
| Sunset Yellow FCF dianion (**1**) |  | –<br>1<br>2<br>4<br>5<br>6<br>7 | 407[a]<br>–<br>–<br>–<br>–<br>–<br>– | 203[b]<br>211[b]<br>219[b]<br>235[b]<br>243[b]<br>251[b]<br>259[b] |
| 6-Hydroxy-5-[(phenyl)azo]-2-naphtalenesulfonate ion (**2**) |  | –<br>1<br>2<br>3<br>4<br>7<br>10 | 327[a]<br>343[a]<br>359[a]<br>375[a]<br>391[a]<br>439[a]<br>487[a] | |
| 2,6-Dihydroxy-5-[(phenyl)azo]-naphtalene (**3**) |  | –<br>1 | 263[a]<br>279[a] | |
| 4-Aminobenzenesulfonate ion (**4**) |  | –<br>1 | 172[a]<br>188[a] | |
| 4-Nitrobenzenesulfonate ion (**5**) |  | –<br>1 | 202[a]<br>218[a] | |
| 4-Hydroxybenzenesulfonate ion (**6**) |  | –<br>1 | 173[a]<br>189[a] | |
| 4-Nitrophenol (**7**) |  | –<br>3 | 138[a]<br>186[a] | |
| 5-Nitro-6-hydroxy-2-naphtalenesulfonate ion (**8**) |  | –<br>1<br>2<br>3 | 268[a]<br>284[a]<br>300[a]<br>316[a] | |
| 6-Hydroxy-2-naphtalenesulfonate ion (**9**) |  | – | 223[a] | |
| 5-Amino-2,6-dihydroxy-naphtalene (**10**) |  | –<br>1<br>2<br>3<br>4<br>5 | 174[a]<br>190[a]<br>206[a]<br>222[a]<br>238[a]<br>254[a] | |

Table 4 (*Continued*)

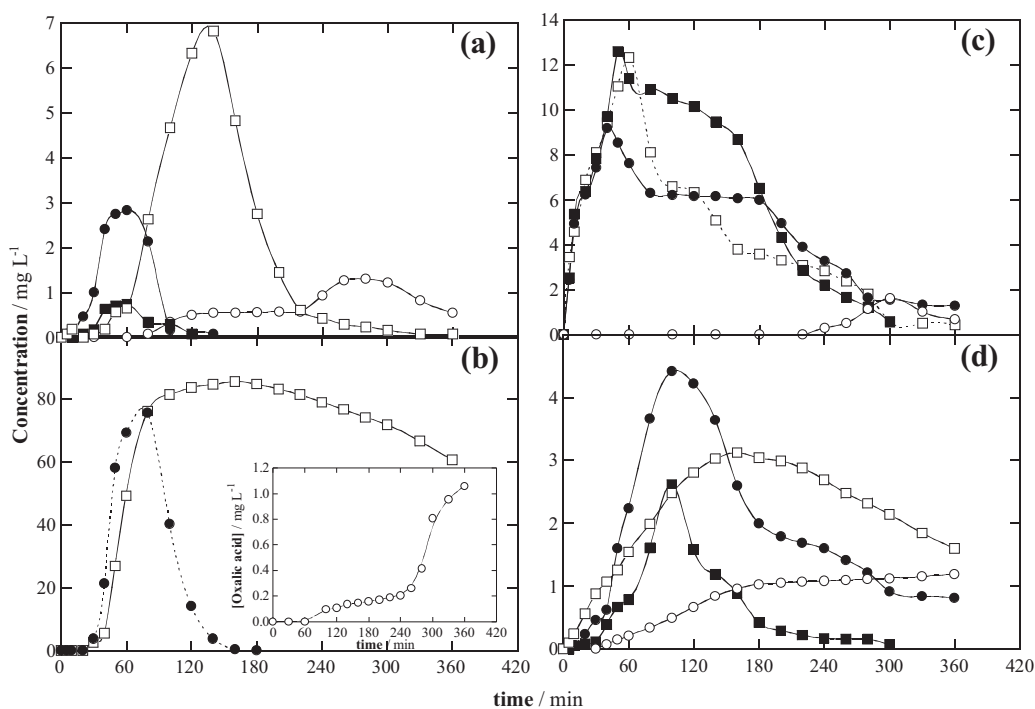| Compound | Molecular formula | Number of –OH added | m/z |
|---|---|---|---|
| 5-Nitro-2,6-dihydroxy-naphtalene (**11**) | | – | 204[a] |
| | | 1 | 220[a] |
| 4-Sulfophthalic acid (**12**) | | – | 245[a] |
| | | 1 | 261[a] |
| 3-Amino-4-hydroxyphthalic acid (**13**) | | – | 196[a] |
| | | 1 | 212[a] |
| | | 2 | 228[a] |
| 3-Nitro-4-hydroxyphthalic acid (**14**) | | – | 226[a] |
| | | 1 | 242[a] |
| | | 2 | 258[a] |
| Phthalic acid (**15**) | | – | 165[a] |
| | | 3 | 213[a] |
| | | 4 | 229[a] |

[a] Negative ions detected with $z = 1$.
[b] Negative ions detected with $z = 2$.



**Fig. 5.** Evolution of (a) tartronic, (b) oxalic, (c) formic and (d) oxamic acids detected during the treatment of 100 mL of 290 mg L$^{-1}$ SY solutions under the conditions of Fig. 1. Method: (○) AO-H$_2$O$_2$, (□) EF, (●) PEF and (■) SPEF.

the low reaction rate of Fe(III)–oxalate complexes with BDD($\bullet$OH). In contrast, these species are totally photolyzed by UVA light after 180 min of PEF. The photolysis rate of Fe(III)–oxalate complexes becomes so fast under solar radiation that they were not detected by SPEF. However, Fig. 5c shows a different trend for formic acid, which is very poorly accumulated and destroyed with BDD($\bullet$OH) in AO-$H_2O_2$, but more largely accumulated and rapidly removed in a similar way by EF, PEF and SPEF, as expected if Fe(III)–formate complexes are oxidized with BDD($\bullet$OH) but poorly photolyzed. Fig. 5d highlights the existence of a slow destruction of oxamic acid with BDD($\bullet$OH) in AO-$H_2O_2$, but, in turn, Fe(III)–oxamate complexes are more rapidly removed with BDD($\bullet$OH) in EF, whereas these complexes are slowly photolyzed in PEF and slightly more rapidly photodecomposed in SPEF, where they disappear in 300 min.

From the aforementioned findings, one can infer that SPEF is the most powerful EAOP for SY mineralization because sunlight can rapidly photolyze oxidation products like Fe(III) complexes of tartronic and oxalic acids, owing to the incapacity of $\bullet$OH to remove these recalcitrant compounds in AO-$H_2O_2$ and EF. A simple mass balance of organic carbon at the end of all treatments (see Figs. 2 and 5) reveals that in AO-$H_2O_2$ the final solution contains $0.9\,mg\,L^{-1}$ TOC related to carboxylic acids, much lower than $31.5\,mg\,L^{-1}$ TOC due to unidentified recalcitrant products that are the major components since they are attacked very slowly by BDD($\bullet$OH). In contrast, the final solution using EF is more largely degraded by $\bullet$OH and is preferentially composed of oxalic acid ($16.2\,mg\,L^{-1}$ TOC) and in much smaller extent of other carboxylic acids ($0.6\,mg\,L^{-1}$ TOC) and unidentified compounds ($2.8\,mg\,L^{-1}$ TOC), which can be hardly removed by BDD($\bullet$OH), but not by $\bullet$OH. The quick photodecarboxylation of Fe(III)–oxalate species by UVA light in PEF and sunlight in SPEF (see Fig. 5b) causes the faster TOC abatement using both methods compared with EF. However, the most persistent formic and oxamic acids are present in solution even after 240 and 150 min of PEF and SPEF (see Fig. 2), giving rise to a total TOC of 1.3 and $2.6\,mg\,L^{-1}$ (see Fig. 5c and d), respectively. That means that the final solutions treated by PEF and SPEF still contain 3.9 and $6.8\,mg\,L^{-1}$ TOC of by-products, respectively, that are even more recalcitrant than carboxylic acids since they can be very difficultly destroyed by $\bullet$OH, but not photolyzed.

The mineralization of azo dyes usually involves the release of their nitrogen and sulfur atoms in the form of inorganic ions such as $NH_4^+$, $NO_3^-$ and $SO_4^{2-}$ [4,9,44,46]. Quantification of inorganic nitrogen ions formed after 360 min of the treatment of $290\,mg\,L^{-1}$ SY solutions by all EAOPs at $33.3\,mA\,cm^{-2}$ was attempted by ionic chromatography. However, this technique did not allow the detection of $NO_3^-$ and $NO_2^-$ ions, only being found very low concentrations of $NH_4^+$ ion ($<1\,mg\,L^{-1}$). The TN analysis of such electrolyzed solutions confirmed that the initial N of $14.6\,mg\,L^{-1}$ was drastically reduced to $3–4\,mg\,L^{-1}$ in all EAOPs. This suggests the release of the major part of the initial N (73–79%) from the solution during all mineralization processes, probably as $N_2$ and $N_xO_y$ species, while the rest of N forms primordially recalcitrant unidentified N-derivatives that remain in the final solutions. On the other hand, to confirm the generation of $SO_4^{2-}$ ion, a $290\,mg\,L^{-1}$ SY solution ($33.3\,mg\,L^{-1}$ of initial S) in 0.05 M $LiClO_4$ with 0.5 mM $FeSO_4\cdot7H_2O$ at pH 3.0 (adjusted with $HClO_4$) was electrolyzed by SPEF at $33.3\,mA\,cm^{-2}$ and $35\,^{\circ}C$. Under these conditions, TOC was reduced by 96% in 240 min, but all the initial S was released as $SO_4^{2-}$ ion (about $100\,mg\,L^{-1}$) in only 80 min, indicating that this ion is formed from all sulfonated derivatives at the first stages of the process.

### 3.4. SPEF treatment of SY at the 10 L solar pre-pilot plant

The degradation of SY was scaled-up to pre-pilot scale for SPEF, the most powerful EAOP tested. Since organic matter is destroyed

mainly by $\bullet$OH in the bulk and UV radiation, a Pt/carbon–PTFE air-diffusion cell was used in the pre-pilot plant because it yielded much lower $E_{cell}$ values than a BDD/carbon–PTFE air-diffusion cell, then substantially reducing the energy consumption for each $j$. The experiments were made by electrolyzing 10 L of a $290\,mg\,L^{-1}$ SY solution in 0.05 M $Na_2SO_4$ with 0.5 mM $Fe^{2+}$ at pH 3.0 and $35\,^{\circ}C$ in the pre-pilot plant coupled with a solar CPCs photoreactor by applying 33.2, 55.4 and $77.6\,mA\,cm^{-2}$ to the Pt/air-cell, with $E_{cell}$ values of 5.3, 7.7 and 9.5 V, respectively. In all these trials, the solution pH dropped slowly to final values of 2.8–2.9 and it was regulated by adding 50% (w/v) NaOH.

Fig. 6a depicts the time course of the percentage of color removal at $\lambda_{max} = 482\,nm$ for the above electrolytic trials. As expected, this parameter rose with increasing $j$ by the greater production of
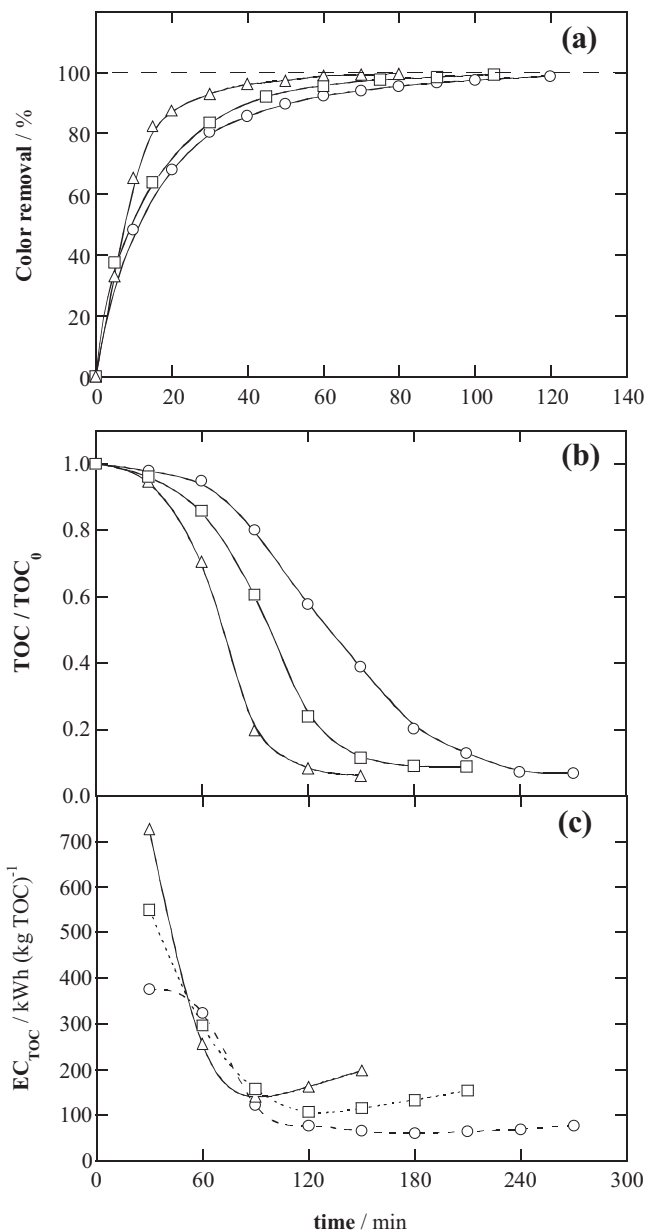


**Fig. 6.** Effect of current density on the change of (a) percentage of color removal at $\lambda_{max} = 482\,nm$, (b) normalized TOC removal and (c) energy consumption per unit TOC mass with electrolysis time for the SPEF treatment of 10 L of a $290\,mg\,L^{-1}$ SY solution in 0.05 M $Na_2SO_4$ with 0.5 mM $Fe^{2+}$ at pH 3.0 and $35\,^{\circ}C$ in a pre-pilot plant connected to a solar CPCs photoreactor (irradiated volume 1.57 L) and equipped with a Pt/carbon–PTFE air-diffusion cell with electrodes of $90.2\,cm^2$ area. Applied current density: ($\bigcirc$) $33.2\,mA\,cm^{-2}$, ($\square$) $55.4\,mA\,cm^{-2}$ and ($\triangle$) $77.6\,mA\,cm^{-2}$.

Pt($^{\bullet}$OH) and $^{\bullet}$OH in the bulk. Total decolorization was thus achieved at shorter times of 120, 100 and 80 min for increasing $j$ of 33.2, 55.4 and 77.6 mA cm$^{-2}$. The corresponding $k_1$(dec) values are given in Table 2. Comparison of Fig. 1 and 6c for SPEF, as well as of $k_1$(dec) values obtained for the 100 mL cell and 10 L solar pre-pilot plant at near 33 mA cm$^{-2}$, indicates that SY decolorization is much faster in the former system. This is not surprising in view of the different experimental conditions used in both cases. Since the electrode area/solution volume ratio is 30 cm$^2$ L$^{-1}$ for the 100 mL cell and 9 cm$^2$ L$^{-1}$ for the 10 L solar pre-pilot plant, one may expect an acceleration of 30/9 = 3.33 times for the decolorization rate of the former respect to the latter. This is in good agreement with the increase in 2.65-fold of $k_1$(dec) found for the 100 mL cell (see Table 2), corroborating that $^{\bullet}$OH is the main oxidant of SY and its colored aromatic products in the 10 L solar pre-pilot plant, with small participation of Pt($^{\bullet}$OH). Besides, other aspects related to solar radiation could influence the efficiency of the two tested systems such as: (i) the 100 mL cell was totally irradiated by sunlight in contrast to the very low irradiated volume/total volume ratio of 15.7% in the 10 L pre-pilot plan, (ii) the 10 L pre-pilot plant had a better solar irradiation capture system accomplished by CPCs, which can use efficiently direct and diffuse solar irradiation, whereas the 100 mL cell mostly uses the direct irradiation, although a very small part of diffuse UV irradiation reflected by the mirror at the bottom of the cell reached the solution and (iii) while at the 100 mL cell all solar wavelengths reached the solution in direct contact with the atmosphere, the CPCs borosilicate glass tubes exhibits a cut-off of about 285 nm.

The normalized TOC decay shown in Fig. 6b for the same trials also evidences an increase in degradation rate with increasing $j$, attaining an almost total mineralization of 91–94% after 270 min at 33.2 mA cm$^{-2}$, 210 min at 55.4 mA cm$^{-2}$ and 150 min at 77.6 mA cm$^{-2}$. This was also reflected in the gradual rise of $r_0$(TOC) from $1.0 \pm 0.1$ to $1.8 \pm 0.1$ mg L$^{-1}$ min$^{-1}$ in the $j$ range tested (see Table 3). However, more $Q$ was consumed when $j$ rose, reaching final values from 1.35 to 1.75 Ah L$^{-1}$. This means that more $^{\bullet}$OH are formed at greater $j$, but their relative amounts diminish as a result of the increase in rate of their non-oxidizing reactions, as pointed out above in the behavior of the 100 mL cell. Moreover, Fig. 6b also shows that at a given $j$ the mineralization process is gradually accelerated up to about 80% TOC removal, which can be related to the progressive formation of products that can be more rapidly photolyzed by sunlight. This behavior caused a dramatic drop in EC$_{TOC}$ at the beginning of all trials up to minimum values between 90 and 120 min, as can be seen in Fig. 6c. The increase in $j$ caused higher EC$_{TOC}$ values, as expected by the gradual rise in $E_{cell}$. Thus, 77 kWh (kg TOC)$^{-1}$ (7.2 kWh m$^{-3}$) for 33.2 mA cm$^{-2}$, 154 kWh (kg TOC)$^{-1}$ (14.2 kWh m$^{-3}$) for 55.4 mA cm$^{-2}$ and 197 kWh (kg TOC)$^{-1}$ (16.6 kWh m$^{-3}$) for 77.6 mA cm$^{-2}$ were spent for achieving 91–94% mineralization. Note that for the lowest $j$ tested, similar EC$_{TOC}$ values between 60 and 77 kWh (kg TOC)$^{-1}$ were obtained from 120 min to the end of the treatment at 270 min (see Fig. 6c), when a fast TOC abatement took place (see Fig. 6b), while EC increased from 3.2 to 7.1 kWh m$^{-3}$. All these findings demonstrate the viability of SPEF for SY degradation at industrial scale, where low $j$ values are more useful since they yield a more efficient and economic process with lower EC$_{TOC}$, although longer times are needed for reaching almost total mineralization.

The reaction of SY with Pt($^{\bullet}$OH) formed from reaction (1) and mainly $^{\bullet}$OH produced from Fenton's reaction (3) and photolytic reaction (6) was followed by reversed-phase HPLC. Fig. 7a exemplifies the fast decay in azo dye concentration at 77.6 mA cm$^{-2}$ to disappear in 22 min. Nevertheless, the corresponding $k_1$(SY) value, given in Table 2, is even lower than that determined for the 100 mL cell at 33.3 mA cm$^{-2}$ because of the different experimental conditions used in the 10 L solar pre-pilot plant. This pseudo-first-order kinetics suggests again the constant production of oxidant
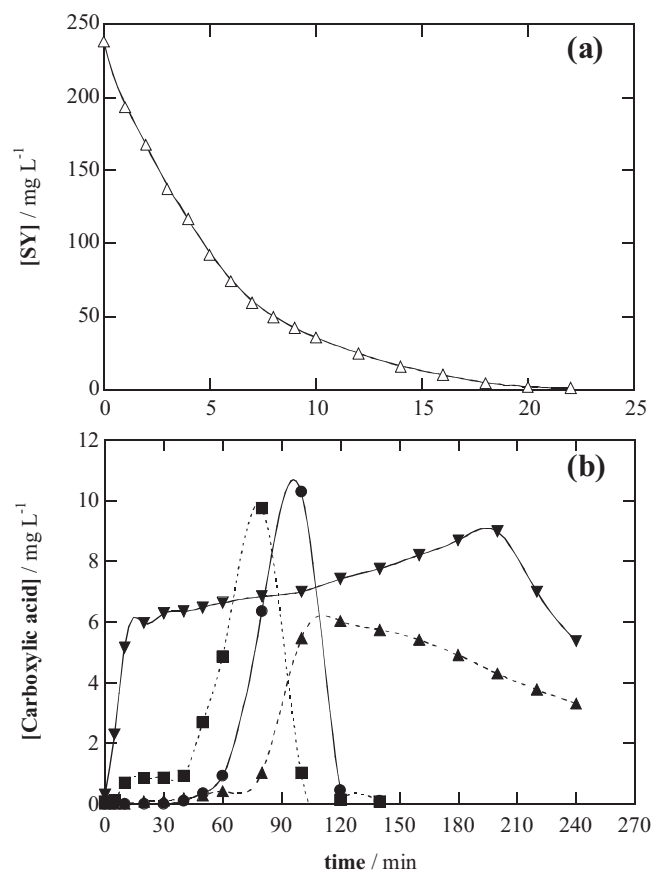


**Fig. 7.** (a) Decay of dye concentration with electrolysis time for the SPEF degradation of 10 L of a 290 mg L$^{-1}$ SY solution under the same conditions of Fig. 6 at 77.6 mA cm$^{-2}$. (b) Time course of (■) tartronic, (●) oxalic, (▼) formic and (▲) oxamic acids detected during the above treatment.

$^{\bullet}$OH in the latter system. Moreover, the same generated carboxylic acids were identified by ion-exclusion HPLC in both electrolytic systems. Fig. 7b shows that at 77.6 mA cm$^{-2}$, both tartronic and oxalic acids were rapidly and completely removed in less than 150 min, as expected from the quick photolysis of their Fe(III) complexes under solar radiation. In contrast, formic and oxamic acids remained in solution, a different behavior to that found for the 100 mL cell with a BDD anode where they were totally degraded (see Fig. 5c and d). After 150 min of electrolysis, these acids contribute largely in 3.6 mg L$^{-1}$ TOC to the remaining solution, also containing 2.0 mg L$^{-1}$ TOC of other unidentified products. That means that Fe(III)–formate and Fe(III)–oxamate complexes are not attacked by Pt($^{\bullet}$OH) and are poorly photolyzed in SPEF. Consequently, in the 100 mL BDD/carbon–PTFE air-diffusion cell they are removed by the more reactive BDD($^{\bullet}$OH). This effect on generated carboxylic acids is the main oxidative difference found in this EAOP when Pt is used instead of a BDD anode, since aromatics are mainly destroyed by $^{\bullet}$OH in the bulk.

### 3.5. Proposed reaction pathway for SY mineralization

Based on the oxidation products detected (see Table 4 and Fig. 5), Fig. 8 presents a general reaction sequence proposed for SY mineralization in acidic medium by the EAOPs tested. In this pathway, M($^{\bullet}$OH) denotes BDD($^{\bullet}$OH) or Pt($^{\bullet}$OH), which attack aromatic products much more slowly than $^{\bullet}$OH. Parallel and slower reaction of products with other ROS (H$_2$O$_2$, HO$_2$$^{\bullet}$) is also feasible. Formation of Fe(III) complexes in EF, PEF and SPEF is only highlighted for the ultimate carboxylic acids for simplicity.
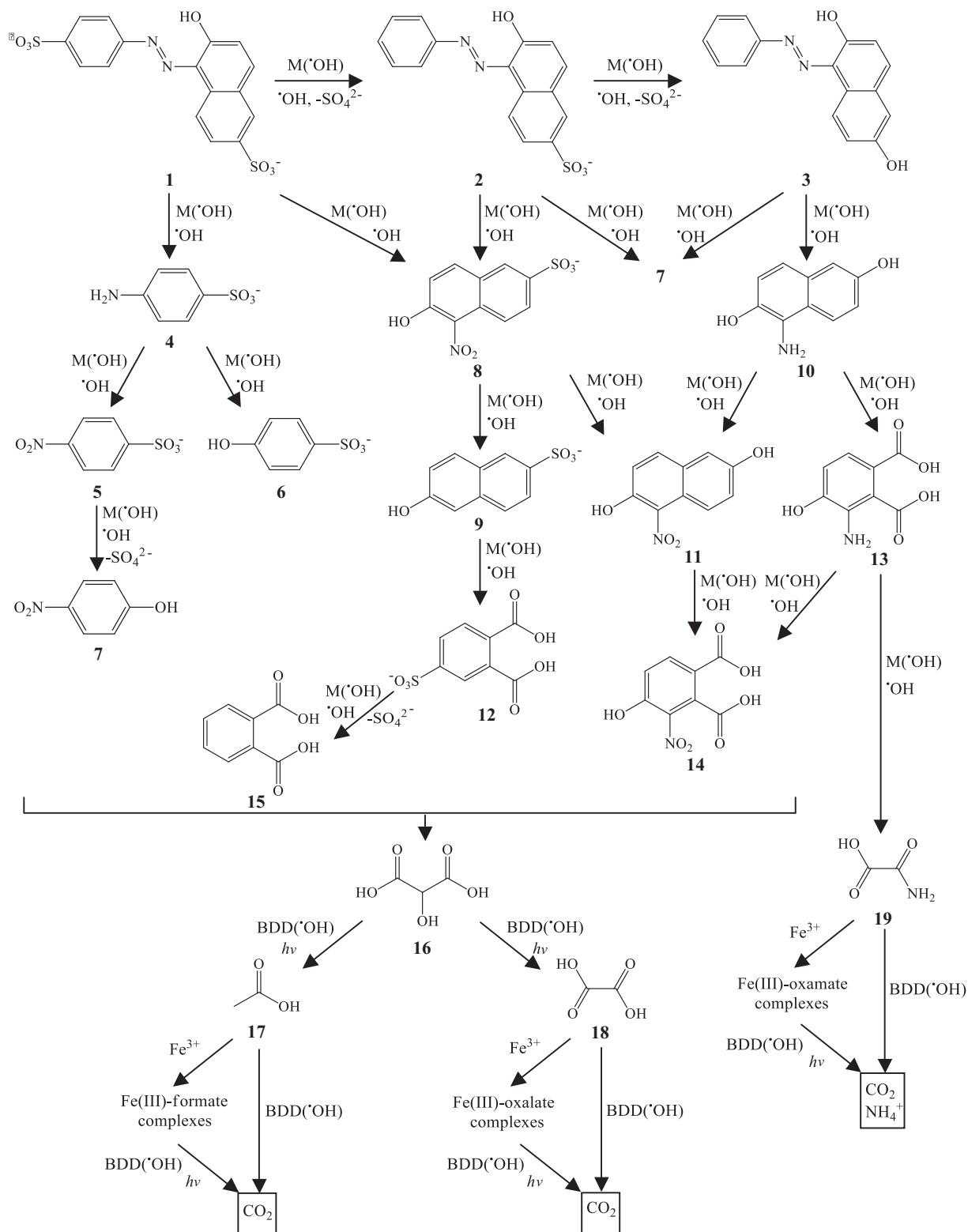
**Fig. 8.** Proposed reaction sequence for the mineralization of Sunset Yellow FCF in acidic medium by EAOPs. M($^{\bullet}$OH) denotes the reactive $^{\bullet}$OH generated either at a Pt or BDD anode, whereas BDD($^{\bullet}$OH) represents this radical on a BDD anode.

The process is initiated either by the desulfonation of **1** to yield **2** or the cleavage of its —N=N— bond giving the benzenic compound **4** and the naphthalenic compound **8**. Further desulfonation of **2** leads to **3**. Compound **4** is subsequently either oxidized to **5**, which is desulfonated to **7**, or hydroxylated to **6**. The benzenic compound **7** can also be formed from the cleavage of the azo bond of **2** and **3**,

which also produce the naphthalenic derivatives **8** and **10**, respectively. The degradation of **8** yields **15** via denitration to **9** followed by opening of its naphthalenic ring to **12**. Compound **10** is oxidized to **11** or **13**, which are then transformed into **14**. Compound **11** can also be formed from desulfonation and hydroxylation of **8**. Further oxidation of benzenic and phthalic acid derivatives with ring

opening leads to shorter aliphatic products like carboxylic acids. Thus, compounds without heteroatoms like **15** evolve to acids **16**–**18**, whereas N-derivatives with a −$NH_2$ group like **13** can produce the ultimate acid **19**. Acid **16** is oxidized to the ultimate acids **17** and **18**. All these ultimate acids can then be slowly mineralized with BDD($\cdot$OH) in AO-$H_2O_2$, but they form Fe(III) complexes in EF, PEF and SPEF that react with this radical and/or are photolyzed by UVA light or solar radiation. While Fe(III)–oxalate complexes are rapidly photodecomposed, Fe(III)–formate and Fe(III)–oxamate species are mainly destroyed by BDD($\cdot$OH).

## 4. Conclusions

A slow decolorization of a 290 mg $L^{-1}$ SY solution at pH 3.0 was achieved in a 100 mL BDD/carbon–PTFE air-diffusion cell using AO-$H_2O_2$ because of its low reaction rate with BDD($\cdot$OH). EF, PEF and SPEF treatments led to a much faster and total decolorization at similar rate due to the quicker oxidation by $\cdot$OH in the bulk. The relative oxidation power of the EAOPs increased in the sequence: AO-$H_2O_2$ < EF < PEF < SPEF. An almost total mineralization with 93–95% TOC removal at 33.3 mA $cm^{-2}$ was only achieved using PEF and SPEF by virtue of the quick photolysis of several Fe(III)–carboxylate species that cannot be removed by $\cdot$OH in EF. The most powerful process was SPEF due to the higher UV intensity supplied by sunlight. The little oxidation action of BDD($\cdot$OH) yielded a poor mineralization in AO-$H_2O_2$. Greater $j$ increased the mineralization rate of SY in all EAOPs, but with the spent of higher $Q$ due to the acceleration of non-oxidizing reactions of BDD($\cdot$OH) and $\cdot$OH. SY always decayed following a pseudo-first-order reaction, with $k_1$(SY) values also raising in the order: AO-$H_2O_2$ < EF < PEF < SPEF, evidencing the production of $\cdot$OH induced by the photolytic reaction (6). SY was more rapidly removed than decolorized indicating that decolorization involves the destruction of colored aromatic products that absorb at the same $\lambda_{max}$ = 482 nm as the azo dye. Up to 14 aromatic products and 34 hydroxylated derivatives, including benzenic, naphthalenic and phthalic acid compounds, were detected by LC–MS. Ion-exclusion HPLC revealed a slow removal of generated carboxylic acids with BDD($\cdot$OH), a rapid photodecomposition of Fe(III)–tartronate and Fe(III)–oxalate complexes by UV light and a gradual destruction of Fe(III)–formate and Fe(III)–oxamate species with BDD($\cdot$OH). While all initial S was converted into $SO_4^{2-}$ ion, the major part of initial N was released from the solution and a minor fraction of it was mineralized to $NH_4^+$. The use of a pre-pilot plant with a Pt/carbon–PTFE air-diffusion cell coupled with a CPCs photoreactor demonstrated the viability of SPEF at industrial scale since it allowed the complete decolorization and almost total mineralization of 10 L of a 290 mg $L^{-1}$ SY solution at pH 3.0. The increase in $j$ from 33.2 to 77.6 mA $cm^{-2}$ gave 91–94% mineralization at shorter times from 270 to 150 min, but with greater $EC_{TOC}$. SY also verified a pseudo-first-order decay, but Fe(III) complexes of formic and oxamic acids remained in solution because they were not removed by Pt($\cdot$OH), this being the main oxidative difference observed when a Pt anode is used instead of BDD in SPEF. Application of low $j$ values are more useful in SPEF since they provide a more efficient and economic process with lower $EC_{TOC}$, although longer times are needed for reaching almost total mineralization.

## Acknowledgements

## Appendix A. Supplementary data

Supplementary data associated with this article can be found, in the online version, at http://dx.doi.org/10.1016/j.apcatb.2013.03.023.

## References

[1] H. Zollinger, Color Chemistry: Syntheses, Properties, and Applications of Organic Dyes and Pigments, VHCA and Wiley-VCH, Switzerland, 2003.
[2] K. Hunger (Ed.), Industrial Dyes Chemistry, Properties, Applications, Wiley-VCH, Germany, 2003.
[3] E. Forgacs, T. Cserháti, G. Oros, Environment International 30 (2004) 953–971.
[4] C.A. Martínez-Huitle, E. Brillas, Applied Catalysis B: Environmental 87 (2009) 105–145.
[5] K.P. Sharma, S. Sharma, S. Sharma, P.K. Singh, S. Kumar, R. Grover, P.K. Sharma, Chemosphere 69 (2007) 48–54.
[6] A.B. Santos, F.J. Cervantes, J.B. van Lier, Bioresource Technology 98 (2007) 2369–2385.
[7] C.A. Martínez-Huitle, S. Ferro, Chemical Society Reviews 35 (2006) 1324–1340.
[8] M. Panizza, G. Cerisola, Chemical Reviews 109 (2009) 6541–6569.
[9] E. Brillas, I. Sirés, M.A. Oturan, Chemical Reviews 109 (2009) 6570–6631.
[10] A. Anglada, A. Urtiaga, I. Ortiz, Journal of Chemical Technology & Biotechnology 84 (2009) 1747–1755.
[11] B. Marselli, J. Garcia-Gomez, P.A. Michaud, M.A. Rodrigo, Ch. Comninellis, Journal of the Electrochemical Society 150 (2003) D79–D83.
[12] P.A. Michaud, M. Panizza, L. Ouattara, T. Diaco, G. Foti, Ch. Comninellis, Journal of Applied Electrochemistry 33 (2003) 151–154.
[13] M. Hamza, R. Abdelhedi, E. Brillas, I. Sirés, Journal of Electroanalytical Chemistry 627 (2009) 41–50.
[14] C. Flox, C. Arias, E. Brillas, A. Savall, K. Groenen-Serrano, Chemosphere 74 (2009) 1340–1347.
[15] M. Faouzi, P. Cañizares, A. Gadri, J. Lobato, B. Nasr, R. Paz, M.A. Rodrigo, C. Saez, Electrochimica Acta 52 (2006) 325–331.
[16] L.S. Andrade, L.A.M. Ruotolo, R.C. Rocha-Filho, N. Bocchi, S.R. Biaggio, J. Iniesta, V. García-Garcia, V. Montiel, Chemosphere 66 (2007) 2035–2043.
[17] E. Butrón, M.E. Juárez, M. Solis, M. Teutli, I. González, J.L. Nava, Electrochimica Acta 52 (2007) 6888–6894.
[18] M. Panizza, G. Cerisola, Journal of Hazardous Materials 153 (2008) 83–88.
[19] E. Brillas, S. Garcia-Segura, M. Skoumal, C. Arias, Chemosphere 79 (2010) 605–612.
[20] J. Sun, H. Lu, L. Du, H. Lin, H. Li, Applied Surface Science 257 (2011) 6667–6671.
[21] J.M. Aquino, M.A. Rodrigo, R.C. Rocha-Filho, C. Sáez, P. Cañizares, Chemical Engineering Journal 184 (2012) 221–227.
[22] S. Garcia-Segura, E. Brillas, Water Research 45 (2011) 2975–2984.
[23] E. Rosales, M. Pazos, M.A. Longo, M.A. Sanromán, Chemical Engineering Journal 155 (2009) 62–67.
[24] S. Hammami, N. Oturan, N. Bellakhal, M. Dachraoui, M.A. Oturan, Journal of Electroanalytical Chemistry 610 (2007) 75–84.
[25] A. Özcan, Y. Şahin, A.S. Koparal, M.A. Oturan, Applied Catalysis B: Environmental 89 (2009) 620–626.
[26] I. Sirés, N. Oturan, M.A. Oturan, Water Research 44 (2010) 3109–3120.
[27] M.A. Oturan, N. Oturan, M.C. Edelahi, F.I. Podvorica, K. El Kacemi, Chemical Engineering Journal 171 (2011) 127–135.
[28] M. Zhou, Q. Tan, Q. Wang, Y. Jiao, N. Oturan, M.A. Oturan, Journal of Hazardous Materials 215–216 (2012) 287–293.
[29] A. Özcan, Y. Sahin, A.S. Koparal, M.A. Oturan, Journal of Electroanalytical Chemistry 616 (2008) 71–78.
[30] K. Cruz-González, O. Torres-López, A.M. García-León, E. Brillas, A. Hernández-Ramírez, J.M. Peralta-Hernández, Desalination 286 (2012) 63–68.
[31] C. Ramírez, A. Saldaña, B. Hernández, R. Acero, R. Guerra, S. Garcia-Segura, E. Brillas, J.M. Peralta-Hernández, Journal of Industrial and Engineering Chemistry 19 (2013) 571–579.
[32] E. Brillas, B. Boye, M.A. Baños, J.C. Calpe, J.A. Garrido, Chemosphere 51 (2003) 227–235.
[33] S. Ammar, R. Abdelhedi, C. Flox, C. Arias, E. Brillas, Environmental Chemistry Letters 4 (2006) 229–233.
[34] I. Sirés, F. Centellas, J.A. Garrido, R.M. Rodríguez, C. Arias, P.L. Cabot, E. Brillas, Applied Catalysis B: Environmental 72 (2007) 373–381.
[35] R. Salazar, S. Garcia-Segura, M.S. Ureta-Zañartu, E. Brillas, Electrochimica Acta 56 (2011) 6371–6379.
[36] R. Salazar, E. Brillas, I. Sirés, Applied Catalysis B: Environmental 115–116 (2012) 107–116.

[37] A. Wang, J. Qu, H. Liu, J. Ru, Applied Catalysis B: Environmental 84 (2008) 393–399.
[38] M. Zarei, A.R. Khataee, R. Ordikhani-Seyedlar, M. Fathinia, Electrochimica Acta 55 (2010) 7259–7265.
[39] A.R. Khataee, M. Safarpour, M. Zarei, S. Aber, Journal of Electroanalytical Chemistry 659 (2011) 63–68.
[40] M. Iranifam, M. Zarei, A.R. Khataee, Journal of Electroanalytical Chemistry 659 (2011) 107–112.
[41] C. Flox, J.A. Garrido, R.M. Rodríguez, P.L. Cabot, F. Centellas, C. Arias, E. Brillas, Catalysis Today 129 (2007) 29–36.
[42] W.-P. Ting, M.-C. Lu, Y.-H. Huang, Journal of Hazardous Materials 156 (2008) 421–427.
[43] S. Garcia-Segura, L.C. Almeida, N. Bocchi, E. Brillas, Journal of Hazardous Materials 194 (2011) 109–118.
[44] E.J. Ruiz, C. Arias, E. Brillas, A. Hernández-Ramírez, J.M. Peralta-Hernández, Chemosphere 82 (2011) 495–501.
[45] L.C. Almeida, S. Garcia-Segura, N. Bocchi, E. Brillas, Applied Catalysis B: Environmental 103 (2011) 21–30.
[46] S. Garcia-Segura, A. El-Ghenymy, F. Centellas, R.M. Rodríguez, C. Arias, J.A. Garrido, P.L. Cabot, E. Brillas, Journal of Electroanalytical Chemistry 681 (2012) 36–43.
[47] D.M. Marmion, Handbook of U.S. Colorants: Foods, Drugs, Cosmetics, and Medical Devices, John Wiley & Sons, NY, USA, 1991.
[48] C.T. Fragoso, R. Battisti, C. Miranda, P.C. Jesus, Journal of Molecular Catalysis A: Chemical 301 (2009) 93–97.
[49] A.H. Gemeay, A.-F.M. Habib, M.A. Borhan El-Din, Dyes and Pigments 74 (2007) 458–463.
[50] S. Lodha, A. Jain, V. Sharma, P.B. Punjabi, Indian Journal of Chemistry Section A 47A (2008) 397–400.
[51] K. Chanderia, S. Kumar, J. Sharma, R. Ameta, P.B. Punjabi, Arabian Journal of Chemistry (2012) http://dx.doi.org/10.1016/j.arabjc.2012.07.023
[52] M.M. Ghoneim, H.S. El-Desoky, N.M. Zidan, Desalination 274 (2011) 22–30.
[53] B. Boye, M.M. Dieng, E. Brillas, Electrochimica Acta 48 (2003) 781–790.
[54] E. Brillas, M.A. Baños, S. Camps, C. Arias, P.L. Cabot, J.A. Garrido, R.M. Rodríguez, New Journal of Chemistry 28 (2004) 314–322.
[55] S. Raghu, C. Ahmed Basha, Journal of Hazardous Materials 149 (2007) 324–330.
[56] M. Stylidi, D.I. Kondarides, X.E. Verykios, Applied Catalysis B: Environmental 40 (2003) 271–286.
[57] A. Lopez, A. Bozzi, G. Mascolo, J. Kiwi, Journal of Photochemistry and Photobiology A: Chemistry 156 (2003) 121–126.